Deep UV light induced, fast reconfigurable and fixed waveguides in Mg doped $LiTaO_3$

Flurin Juvalta[1], Bozena Koziarska-Glinka[1], Mojca Jazbinšek[1], Germano Montemezzani[1,2], Kenji Kitamura[3] and Peter Günter[1]

[1]*Nonlinear Optics Laboratory, Swiss Federal Institute of Technology, ETH Zurich, CH-8093 Zurich (Switzerland)*
[2]*Laboratoire Matériaux Optiques, Photonique et Systèmes (UMR CNRS 7132), University of Metz and Supélec, 2 rue E. Belin, 57070 Metz (France)*
[3]*Advanced Materials Laboratory, National Institute for Material Science, 1-1 Namiki, Tsukuba, 305-0044 (Japan)*
flurin@phys.ethz.ch

Abstract: Dynamic waveguides are induced beneath the surface of magnesium doped near-stoichiometric lithium tantalate by deep UV light at λ = 257 nm using the interband photorefractive effect. The waveguides can be reconfigured in 10 ms at UV intensities of 100 mW/cm^2. We show the importance of the background illumination for the build-up of dynamic optical waveguides. We also present a new fixing process of the light-induced waveguide structures when the background light is absent. These quasi-fixed structures with dark decay times of several days are due to charges trapped in deep traps.

OCIS codes: (190.5330) Photorefractive nonlinear optics; (230.7370) Waveguides; (260.7190) Ultraviolet.

References and links

1. P. Günter, *Nonlinear Optical Effects and Materials* (Springer Series in Optical Science, Vol. 72, Berlin Heidelberg New York 2000).
2. O. Matoba, T. Inujima, T. Shimura, K. Kuroda, "Segmented photorefractive waveguides in $LiNbO_3$:Fe," J. Opt. Soc. Am. B **15**, 2006–2012 (1998).
3. P. Dittrich, G. Montemezzani, P. Bernasconi, and P. Günter, "Fast, reconfigurable light-induced waveguides," Opt. Lett. **24**, 1508–1510 (1999).
4. P. Zhang, J. Zhao, D. Yang, B. Li, C. Xu,"Optically induced photorefractive waveguides in KNSBN:Ce crystal," Opt. Mat. **23**, 199–303 (2003).
5. J. W. Fleischer, M. Segev, N. K. Efremidis, D. N. Christodoulides, "Observation of two-dimensional discrete solitons in optically induced nonlinear photonic lattices," Nature, **422**, 147–150 (2003).
6. A. Bruner, D. Eger, S. Ruschin , "Second-harmonic generation of green light in periodically poled stoichiometric $LiTaO_3$ doped with MgO," J. Appl. Phys. **96**, 7225–7448 (2004).
7. Z. Bai-Gang, Y. Jian-Quan, L. Yang, X. De-Gang, D. Xin, W. Peng, Z. Tie-Li and J. Feng, "High-efficiency single-pass cw quasi-phase-matched frequency doubling based on PP-MgO:SLT," Chinese Phys. **14**, 353-358 (2005).
8. F. Juvalta, M Jazbinšek, P. Günter, K. Kitamura, "Electro-optical properties of near-stoichiometric and congruent lithium tantalate at ultraviolet wavelengths," J. Opt. Soc. Am. B, **23**, 276–281 (2006).
9. Y. W. Liu, K. Kitamura, S. Takekawa, M. Nakamura, Y. Furukawa, and H. Hatano, "Two-color photorefractive properties in near-stoichiometric lithium tantalate crystals," J. Appl. Phys. **95**, 7637–7644 (2004).
10. P. Dittrich, B. Koziarska-Glinka, G. Montemezzani, P. Günter, S. Takekawa, K. Kitamura, and Y. Furukawa, "Deep-ultraviolet interband photorefraction in lithium tantalate," J. Opt. Soc. Am. B **21**, 632–639 (2004).

#72623 - $15.00 USD Received 3 July 2006; accepted 16 August 2006

11. P. Dittrich, G. Montemezzani, M. Habu, M. Matsukura, S. Takekawa, K. Kitamura, P. Günter, "Sub-millisecond interband photorefraction in magnesium doped lithium tantalate," Opt. Comm. **234**, 131-136 (2004).
12. F. Juvalta, P. Dittrich, G. Montemezzani, M. Jazbinsek, P. Günter, S. Takekawa, K. Kitamura,"Holographic gratings in pure and Mg-doped near-stoichiometric $LiTaO_3$ induced by deep-ultraviolet light," Proc. SPIE 6252, in press (2006)
13. Y. Furukawa, K. Kitamura, E. Suzuki, and K. Niwa, "Stoichiometric $LiTaO_3$ single crystal growth by double crucible Czochralski method using automatic powder supply system," J. Crystal Growth **197**, 889–895 (1999).
14. R. Mosimann, D. Haertle, M. Jazbinsek, G. Montemezzani, P. Günter, "Determination of the absorption constant in the interband region by photocurrent measurements," Appl. Phys. B, **83**, 114-119 (2006).
15. P. Günter and J.P. Huignard, *Photorefractive materials and their applications 1: Basic effects* (Springer Verlag, Berlin 2006).
16. P. Bernasconi, G. Montemezzani and P. Günter, "Off-bragg-angle light diffraction and structure of dynamic interband photorefractive gratings," Appl. Phys. B **68**, 833-842 (1999).
17. D. Marcuse,"Modes of a symmetric slab optical waveguide in birefringent media," IEEE J. Quantum Electron. **14**, 736-741 (1978).

1. Introduction

Optical waveguides are one of the fundamental building blocks for integrated optical applications and devices such as modulators, filters, switches and couplers [1]. In nonlinear optical applications like harmonic generation or parametric mixing, guiding the light allows maintaining a high intensity over a much longer interaction length leading to larger conversion efficiencies as in bulk materials. There are many techniques for fabricating permanent waveguides including ion in-diffusion, ion exchange, ion implantation, fs laser ablation, photolithography and epitaxial thin film deposition. By using these techniques, a permanent change of the refractive index in the waveguide region is obtained. This precludes an easy reconfiguration of the waveguide structure. Recently, several techniques based on light-induced refractive index chances in photorefractive materials have been developed [2, 3, 4, 5]. One of the advantage of such optically induced waveguides is that they can be reconfigured solely by changing the light illumination. For applications such as optical switching, optical routing or dynamic optical interconnections, fast reconfigurable waveguides are required, which can be easily achieved with the light induced techniques.

A promising material for frequency doubling[6, 7], electro-optics[8], long-persistent holographic storage[9] and interband photorefraction[10] is near-stoichiometric and/or Mg-doped $LiTaO_3$, that is transparent down to UV wavelengths near λ = 260 nm. The advantage of this material compared to the as-grown congruent $LiTaO_3$ for the above mentioned applications is the greatly reduced concentration of intrinsic trap levels that are responsible for the conventional photorefractive effect.[6]$^{-}$[10] We demonstrate here the fabrication of light-induced waveguides in magnesium doped near-stoichiometric lithium tantalate (Mg:SLT). We first apply the light-induced technique that was previously used for $KNbO_3$ [3], where the waveguides were produced via interband photorefractive field screening in a biased crystal. The induced waveguides in Mg:SLT are reconfigurable in a fast way using controlling light at λ = 257 nm, with waveguide build-up times of 10 ms at UV intensities of 100 mW/cm^2.

Recently, in Mg:SLT, a quasi-fixing of holographic gratings near the crystal surface was observed using interband illumination [11, 12]. We investigate this quasi-fixing via interband photorefractive measurements in the transverse geometry. We show that this fixing is due to charges trapped in long-lifetime deep traps. We further demonstrate, that the same fixing effect can be used to obtain quasi-fixed waveguide structures in this material. Using such fixing mechanism, in routing and switching applications, an optical interconnection can be maintained without the need of any light illumination. When the connection is no longer required, it can be deleted by simply illuminating the crystal homogeneously, allowing another new connection to be established leading to a new waveguide structure.

#72623 - $15.00 USD Received 3 July 2006; accepted 16 August 2006

2. Experimental

2.1. *Growth and preparation of Mg-doped near-stoichiometric $LiTaO_3$*

We used a magnesium doped near-stoichiometric $LiTaO_3$ crystal (Mg:SLT) grown by one of the coauthors. The crystal growth axis was along *c* using a lithium-rich melt (LiO_2:Ta_2O_5 = 58:42 as mole ratio) using the double crucible Czochralski method equipped with an automatic powder supply system [13]. MgO was added into this Li-rich melt. The grown crystal was poled by applying an electric field along the *c*-axis at a temperature higher than the Curie temperature $T_c = 694.3 \pm 1°C$. The MgO concentration of the grown crystal was 1.0 mol% as determined by Ion coupled Plasma Mass Spectroscopy. The *a* and *b* surfaces and the edges of the crystal were polished from both sides. On the *c* surfaces, silver-paste electrodes were painted for applying the electric field. The crystal length along the *a*-axis (guiding direction) was 7.91 mm, and the distance between the electrodes (*c*-axis) was 9.0 mm.

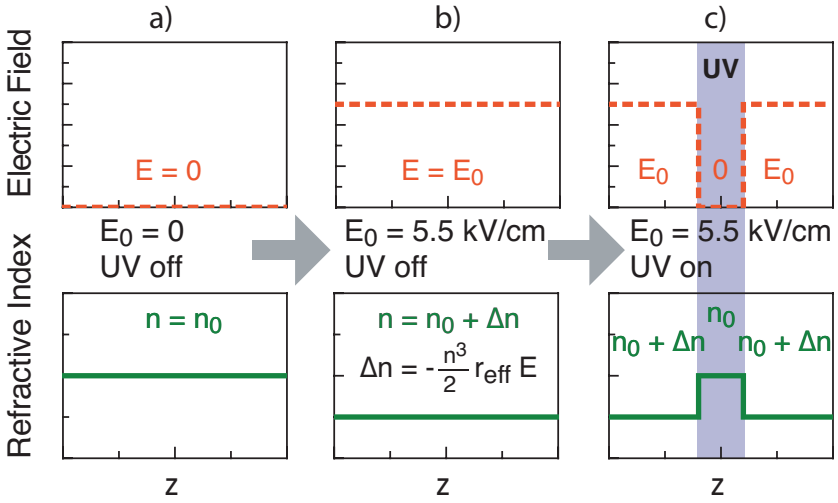

Fig. 1. Simplified electric field and refractive index distribution in a photorefractive crystal for the generation of light induced waveguides by band-to-band excitation:
a) Unperturbed state with refractive index n_0.
b) External field E_0 decreases the refractive index homogeneously by Δn.
c) UV-excited charges screen the external field and produce a waveguide.

2.2. *Light induced waveguides*

In photoconducting electro-optic crystals reconfigurable waveguides are produced by interband photorefraction[3] as explained in the following and as illustrated in Fig. 1. A homogeneous external electric field *E* that is applied to an electro-optic crystal induces a uniform change in the refractive index:

$$\Delta n = -\frac{n^3}{2} r_{\mathrm{eff}} E, \tag{1}$$

where r_{eff} is the effective electro-optic coefficient for the chosen configuration and *n* the refractive index for the corresponding wavelength and polarization. If a small portion of such a biased photorefractive crystal is nonuniformly illuminated, free charge carriers are produced in the bright regions, which screen the applied field due to charge transport and trapping in dark

#72623 - $15.00 USD Received 3 July 2006; accepted 16 August 2006

regions. As a result one gets a strongly reduced electric field in the bright regions, while in dark regions the field is basically unchanged. Via the electro-optic effect, this field distribution generates the refractive index profile, where the refractive index in the dark regions is lowered by Δn. Using a proper field direction and a suitable distribution of the illumination, light induced waveguide structures can be generated in this way. By changing the illumination the waveguide structure can be reconfigured.

By choosing light with photon energy larger than the band-gap energy of the material, charges can be excited directly from one band to the other, i.e. by interband excitation[15]. This process is much more effective in terms of use of the incident photons with respect to a conventional photorefractive effect, where the photoexcitation occurs from dopant or impurity energy levels within the material band gap. In $LiTaO_3$ interband excitation leads to three orders of magnitude faster response compared to conventional trap-level excitation[10]. Due to the strong light absorption at interband wavelengths ($\alpha_z = 690 \pm 40$ cm^{-1} at λ = 257 nm in Mg:SLT which was measured using a thin plate of thickness 100 μm[14]), the screened regions are just underneath the surface. Thus, the waveguides were probed directly beneath the surface, which was possible due to sharp polished crystal edges.

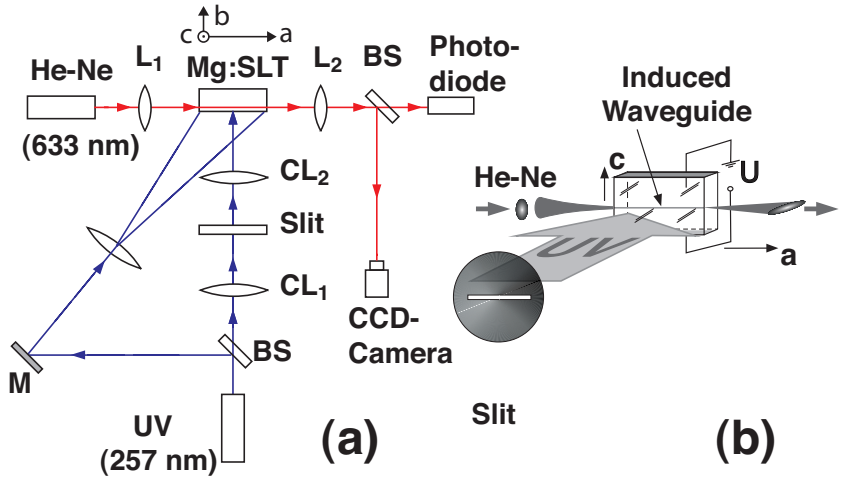

Fig. 2. Top (a) and front (b) views of the experimental set-up for producing light induced waveguides (schematic). L_1 and L_2 are spherical lenses, CL_1 and CL_2 cylindrical lenses, BS beam splitters, M mirror, U the applied voltage.

A schematic view of the experimental set-up to produce light induced waveguides is shown in Fig. 2. An electric field of about 5.5 kV/cm was applied along the *c*-axis of the crystal using silver painted electrodes. A mask with a slit width of 100 μm was homogeneously illuminated by 257 nm UV light polarized parallel to the *c* axis of the crystal. The UV light was provided by an external cavity frequency doubling (WaveTrain, Spectra Physics) of the output of an Ar-ion laser (Innova 200 Coherent Inc.), producing continuous-wave laser radiation at λ = 257 nm with a maximum output power of about 200 mW. The slit was then imaged by the cylindrical lens CL_2 ($f = 75$ mm) onto the *b* surface of the crystal so that the imaged UV stripe had a width of about 20 μm along the *c*-axis and was aligned parallel to the *a*-axis. With a beamsplitter, part of the UV light was separated and after rotating the polarization to avoid interference and expanding the beam, used to homogeneously illuminate the crystal. This background light produced a homogeneous conductivity that permitted a better definition of the narrow stripe region where the external field was screened.

#72623 - $15.00 USD Received 3 July 2006; accepted 16 August 2006

The probe beam from a HeNe laser (633 nm) polarized along the *c*-axis of the crystal was focused by a spherical lens L_1 ($f = 80$ mm) to a waist of 30 μm at the entrance of the waveguide. The exit of the waveguide was imaged by a lens L_2 ($f = 30$ mm) onto a charge-coupled device (CCD) camera and a photodiode. With the photodiode we measured the dynamics of the waveguide while the CCD camera recorded the distribution of the output light. A pinhole was put in front of the photodiode in order to detect the peak intensity I_0 in the center of the readout beam. This intensity increases if the beam is guided in the center. The magnitude of the detected intensity I_0 is a measure of the total power located in the center and is approximately inverse proportional to the waveguide width d.

2.3. Holographic characterization

Light induced charge excitation and recombination processes in photorefractive materials, which are relevant for our light induced waveguide experiments, can be investigated through holographic diffraction experiments [15]. Two light beams that interfere in a photorefractive crystal produce a space charge electric field due to charge excitation in bright regions and recombination in darker regions. This electric field induces a refractive index grating via the electro-optic effect. In conventional photorefraction, charges are excited from mid band-gap levels. When the photon energy of the interfering beams is larger than the band-gap energy of the material, charges can be excited directly from one band to the other. This interband photorefractive effect produces a holographic grating which, in a simplified way, consists of two grating types [16]. Near the surface, where the writing intensity is higher, we obtain gratings for that band-to-band recombination is dominant. At greater depth, where the light intensity is smaller, recombination into traps dominates.

Interband photorefractive effects in Mg:SLT have been previously studied in longitudinal geometry, where the writing beam and the read-out beam enters the crystal from the same surface [10] and the diffracted beam is a mixture of diffraction at different grating compositions along the beam path. The depth structure of an interband photorefractive grating can be determined in the transverse readout geometry, for that the read-out beam is propagating parallel to the input surface of the recording beams. In this geometry, the read-out beam interacts over the whole crystal length with the same grating composition. Therefore the diffraction efficiency, which is defined as the ratio between diffracted and incident light intensities inside the crystal, reflects the grating composition at the depth of propagation and was determined by measuring the diffracted power after the crystal, taking into account Fresnel losses.

3. Results and discussion

3.1. Depth profile of the interband grating in Mg:SLT

Figure 3 shows the result of a holographic measurement in Mg:SLT where the diffraction efficiency was measured for different depths of the readout beam. The grating was written with two UV beams at λ_{UV} = 257 nm and probed with a HeNe-beam. The crystal orientation is depicted on the right side of Fig. 3. The angle between the writing beams was $2\theta_{UV}$ = 16.4° corresponding to a grating spacing of $\Lambda = \lambda_{UV}/(2\sin\theta_{UV})$ = 0.9 μm. The grating was written with a total UV intensity of I_{UV} = 250 mW/cm^2 at the crystal surface. The regions of the two different gratings can be distinguished due to the fact, that in $LiTaO_3$ the trap-dominated grating and the band-dominated grating are mutually phase shifted by π[10, 12]. Therefore the diffracted beams from the two different gratings interfere destructively, which gives rise to the observed minimum of the efficiency profile (open squares in Fig. 3). The shaded areas in Fig. 3 show the dominant regions of the two gratings.

Quasi-fixing of holographic gratings at room temperature in Mg:SLT was recently reported[11, 12]. We measured the depth profile of this quasi-fixed grating after switching off

#72623 - $15.00 USD Received 3 July 2006; accepted 16 August 2006

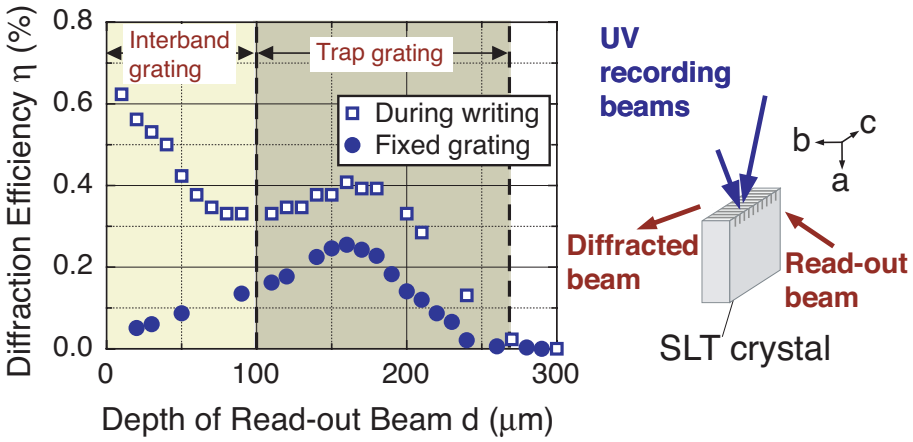

Fig. 3. Left: Diffraction efficiency η as a function of the depth of the readout beam d beneath the illuminated surface measured during recording of the grating (open squares) and after blocking the UV writing beams (filled circles). The shaded regions indicate the interband dominated grating (light shading) and the trap dominated grating (dark shading) as explained in the text. One can clearly see, that the fixed grating is located at the depth of the trap dominated grating. Right: Set-up and crystal orientation for diffraction measurements in the transverse geometry.

both writing beams at the same time. The filled circles in Fig. 3 show the measured diffraction efficiency as a function of the depth of the read-out beam. One can clearly see that the location of this fixed grating corresponds to the location of the trap dominated grating. This indicates that charges excited by the high photon energy UV light are in this region located in deep traps with a longer lifetime and an energy level higher than the photon energy of the readout beam. The lifetime in the dark was estimated to several days, while under permanent read-out with He-Ne light, the fixed grating decayed within 10 hours. Homogeneous illumination with light at lower wavelengths ($\lambda \lesssim 360$ nm) could excite the charges from these deep traps and destroy the fixed structures. A fixing process was also observed in our waveguide experiments with Mg:SLT which we will discuss in section 3.4.

3.2. Waveguide profile

In the light-induced waveguide experiment (Fig. 2), we first measured the beam profile of the read-out beam at the output surface of the crystal. The images are depicted in Fig. 4 for the situations without(left) and with(right) UV stripe illumination. In both cases, an electric field of about 5.5 kV/cm was applied and the crystal was illuminated with a uniform background UV-light with an intensity of approximately 10 mW/cm^2. The UV stripe had an intensity of about 200 mW/cm^2. In absence of the UV stripe, the natural diffraction of the probe beam was observed, which expands to a full width half maximum (FWHM) of about 70 μm (left-hand side). On the right-hand side of Fig. 4, one can clearly distinguish, that the UV stripe produced a waveguide in which the red probe beam was guided. The FWHM of the intensity distribution of the guided waveguide mode was about 17 μm. The central beam profile along the orthogonal axis was not significantly affected by the UV stripe.

The refractive index change for the guided He-Ne light, induced by the UV stripe, can be calculated using Eq. (1). With the refractive indices $n_2 = 2.177$ and $n_3 = 2.175$, the electro-optic coefficients $r_{13} = 8$ pm/V and $r_{33} = 31$ pm/V [8], and the electric field $E_3 = 5.5$ kV/cm, the induced refractive index changes are $\Delta n_2 = -2.3 \times 10^{-5}$ and $\Delta n_3 = -8.8 \times 10^{-5}$ for the two

#72623 - $15.00 USD Received 3 July 2006; accepted 16 August 2006

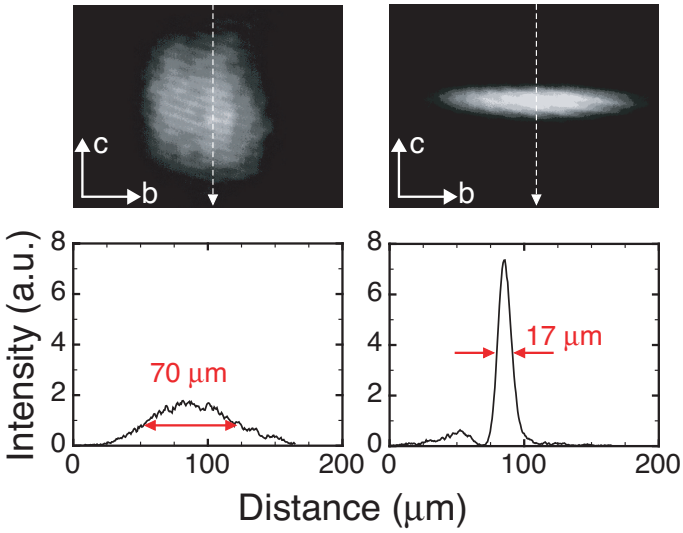

Fig. 4. Top, CCD images of the intensity distribution of the He-Ne probe beam at the exit face of the biased crystal. Bottom, one dimensional beam profiles along the white dashed arrows. The left-side images correspond to the situation with UV illumination off, while for the right side images the UV illumination was on.

polarizations respectively.

We approximate our waveguide with a step-profile planar waveguide. The width of this waveguide corresponds to the width of the imaged UV stripe and was d = 20 μm along the c-axis. With our read-out beam, which is polarized in the c direction, we can excite only TM modes. For this simplified model, the total number of guided TM modes can be calculated with the cutoff condition for the N-th mode(N=1,2,3,...)[17]

$$(N-1)\frac{\pi}{2} = k\frac{d}{2}\frac{n_2}{n_3}\sqrt{n_3^2 - \bar{n}_3^2} \equiv V, \tag{2}$$

where n_2 and n_3 are the refractive indices for light polarized in the b and c direction inside the waveguide (core). The parameters with an overbar belong to the quantities describing the cladding ($\bar{n}_i = n_i + \Delta n_i$). The symbol d represents the waveguide width and k the wavenumber of the probe beam in vacuum.

Applying our values into Eq. (2) we find, that the first two modes should be guided.

The intensity distribution inside the waveguide of the fundamental mode TM_0 of such a waveguide can be described by

$$I(z) = I_0 \cos^2(\kappa z) \qquad z \in [-d/2, d/2] \tag{3}$$

where κ is the solution of the eigenvalue equation for TM modes[17]

$$\tan\left(\frac{\kappa d}{2}\right) = \frac{n_2 n_3}{\bar{n}_2 \bar{n}_3}\sqrt{\left(\frac{2V}{\kappa d}\right)^2 - 1}. \tag{4}$$

From Eq. (3) the full width half maximum of the intensity distribution can be calculated as

$$W_{\mathrm{FWHM}} = \frac{\pi}{2\kappa} \tag{5}$$

#72623 - $15.00 USD Received 3 July 2006; accepted 16 August 2006

Inserting our parameters in the above equations, the fundamental mode TM_0 of our waveguide is expected to have a width of $W_{\mathrm{FWHM}} = 15\ \mu$m, which is in excellent agreement with the measurement.

3.3. Waveguide dynamics

The build-up (τ_b) and decay times (τ_d) of the waveguide structures were determined by opening and closing the UV controlling light. During both processes, the crystal was illuminated with homogeneous background UV light. The times were determined by measuring the transmission of the probe beam through a small pinhole with diameter of about 100μm in the image plane of lens L_2 as shown in Fig. 2a. The transmission through the pinhole was high only if the He-Ne beam was guided inside the crystal and the observed time constants in the transmission dynamics reflect those of the waveguide build-up and decay processes. The build-up of the waveguide structure is therefore characterized by the build-up of the monitored intensity, which can be described with a semi-heuristic double exponential function of the form

$$I = I_1(1-e^{-t/\tau_1}) + I_2(1-e^{-t/\tau_2}). \tag{6}$$

A similar expression describes the decay of the waveguide structure. The fast component I_1 carried about 80% of the intensity and was about one order of magnitude faster than the slow component I_2. Fig. 5a shows the fast component of the waveguide formation and decay processes as a function of the controlling UV-intensity.

The build-up time (τ_b) is the time needed for screening the applied electric field, which is attained by moving charges out of the illuminated region and forming a space-charge field pointing against the initially applied field. In the first approximation the response scales with the dielectric response time

$$\tau_b = \frac{\varepsilon\varepsilon_0}{\sigma_{\mathrm{ph}}} = \frac{\varepsilon\varepsilon_0}{e\mu_e n + e\mu_h p}, \tag{7}$$

where ε is the low-frequency dielectric constant, ε_0 is the permittivity of free space, σ_{ph} is the photoconductivity induced by the UV illumination, defined by the mobilites μ_e and μ_h and the densities n and p of free electrons and holes respectively, and e is the elementary charge. Eq. (7) allows to estimate the induced photoconductivity with the measured build-up times. At UV intensities of 10 mW/cm^2 we get a photoconductivity of about $\sigma_{\mathrm{ph}} = 10^{-8}(\Omega m)^{-1}$. This is the same order of magnitude as the photoconductivity measured in undoped near-stoichiometric $LiTaO_3$ ($\sigma_{\mathrm{ph}} = 3\times 10^{-8}(\Omega m)^{-1}$) [10].

For higher writing intensities, more mobile charge carriers are excited which screen the applied electric field and the screening becomes faster. For band-to-band excitation, the charge densities n and p are equal and grow with the square root of the light intensity[15]. According to Eq. (7), the build-up times are then inverse proportional to the square root of the controlling UV light intensity $\tau_b \propto (I_{UV})^{-0.5}$. Our measured build-up times show also this proportionality as shown in Fig. 5a by the solid line. Therefore, we conclude that the main process for inducing the mobile charge carriers is the interband photorefractive effect where the charges are excited directly from one band into the other by the illumination.

The build-up time at UV intensities of 100 mW/cm^2 was about 10 ms. This is one order of magnitude slower than the build-up of light-induced waveguides in $KNbO_3$ at λ = 364 nm for the same intensity. The absorption constant of $KNbO_3$ at that wavelength is α_z = 540 cm^{-1}, which is comparable to the absorption constant α_z = 690 cm^{-1} in Mg:SLT at 257 nm [3].

In Mg:SLT the decay times are approximately constant for all UV intensities of the controlling light in contrast to $KNbO_3$ where an increase of the decay times was observed [3]. The decay time τ_d depends only on the background intensity. Fig. 5b shows the fast decay

#72623 - $15.00 USD Received 3 July 2006; accepted 16 August 2006

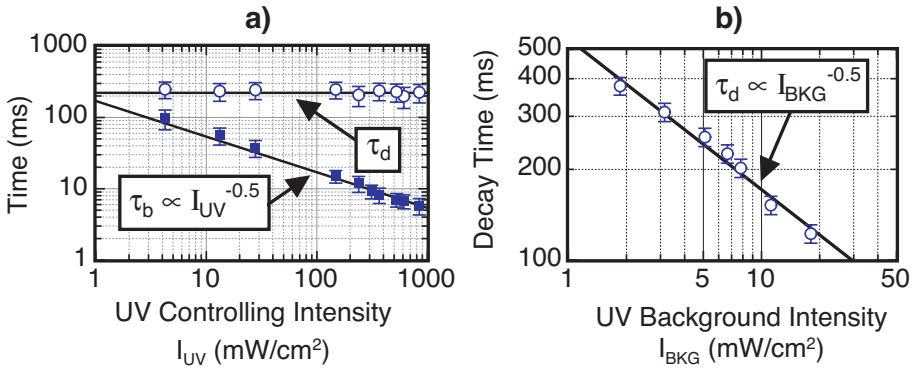

Fig. 5. a) Build-up times (τ_b) and decay times (τ_d) of the light induced waveguides as defined in Eq. (6) for different controlling UV-intensities at the crystal surface. During the decay the crystal was still illuminated with the background UV light of I_{BKG} = 7 mW/cm^2. b) Decay times for different background UV intensities for a fixed controlling light intensity I_{UV} = 100 mW/cm^2.

times for different background intensities for controlling intensity of about 100 mW/cm^2. We found that the decay time is inverse proportional to the square root of the background intensity ($\tau_d \propto I_{BKG}^{-0.5}$). This time dependence can be explained by the fact that the waveguide structures are deleted by the uniform background UV light and that the main process again is the interband photorefractive effect.

3.4. Quasi-fixing of waveguides and double waveguides

An interesting effect was observed without illuminating the crystal with the UV background light, as illustrated in Fig. 6. On the top of Fig. 6 the signal monitored by the photodiode is shown. We distinguish six processes (a) to (f) that are indicated with dashed arrows in the top of Fig. 6, and schematically presented with the refractive index/electric field profiles on the bottom of Fig. 6. These 6 processes are the following:

(a) Initial state: After applying an electric field of about 5.5 kV/cm. The refractive index decreased uniformly over the whole crystal according to Eq.(1).

(b) Waveguide build-up and quasi-fixing: When illuminating the crystal with the UV stripe, the applied electric field is screened by the photoexcited charge carriers, changing the refractive index back to its original value in the illuminated region and a waveguide was formed as theoretically expected. If we blocked the UV controlling light, the waveguides remained partially stable. We attribute this behaviour to the same mechanism responsible for the formation of the quasi-fixed holographic grating discussed in section 3.1. Beyond the edges of the UV stripe, the UV light intensity is weak, therefore the charges can reside in deep traps. The evolution of the quasi-fixed waveguide under continuous readout is shown in Fig. 7a. The fixed structure was stable in the dark over several days, while it decayed under permanent readout with He-Ne light within 10 hours, similar to the decay of the quasi-fixed photorefractive gratings. The fixed structures could be deleted by homogeneous illumination with lower wavelength light ($\lambda \lesssim 360$ nm). This explains why this fixing was not observed when using the background light with wavelength λ = 257 nm.

(c) Widening of the structure: Provided that the crystal is illuminated with the controlling UV stripe further on and the background UV illumination is still absent, the waveguide can widen until roughly the point where the photoconductivity induced by the controlling beam equals the dark conductivity of the material. If the dark conductivity is very weak, as is the

#72623 - $15.00 USD Received 3 July 2006; accepted 16 August 2006

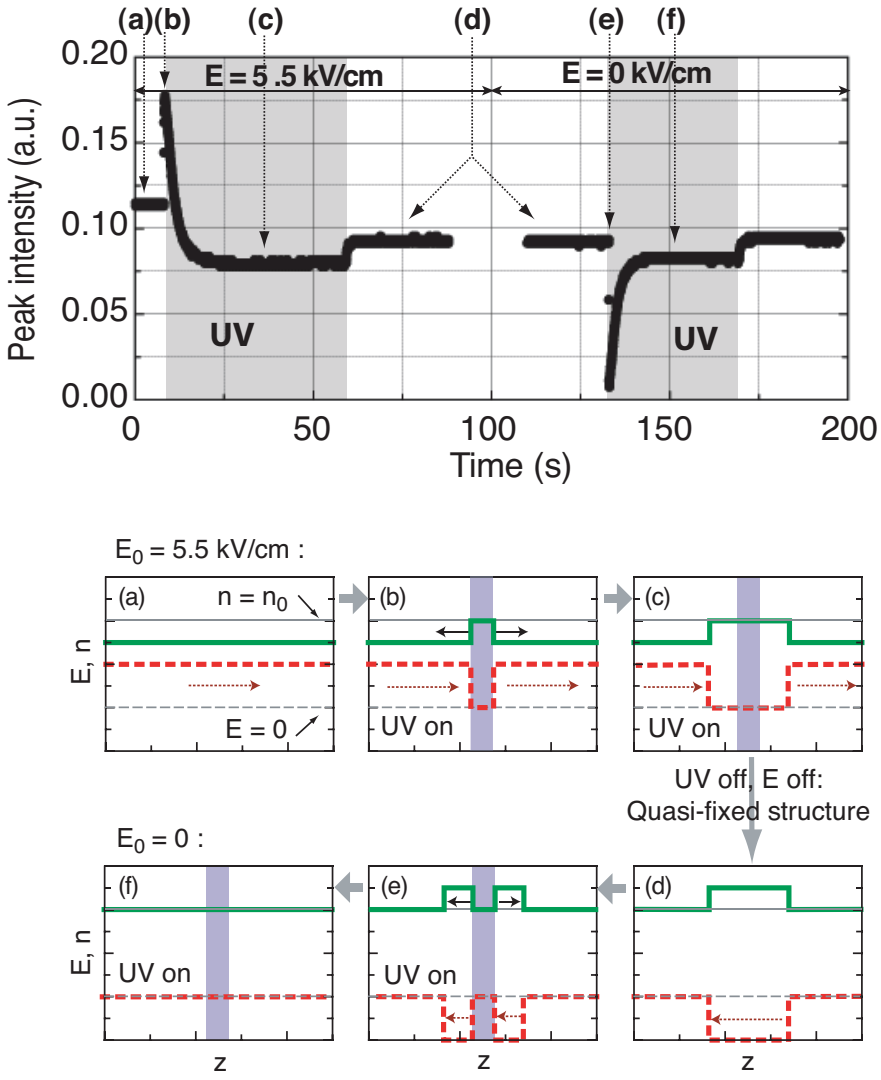

Fig. 6. Top: Peak intensity of the read-out beam at the crystal output surface as a function of time showing the dynamics of waveguide formation in Mg:SLT when the background UV illumination was absent. Bottom: Schematic illustration of the processes (a)-(f) responsible for the observed dynamics. The solid lines represent the change of index profile n, the dashed lines the electric field E. The thin lines indicate $n = n_0$ and $E = 0$, which are the initial values. The dotted arrows point towards the direction of the electric field, while the solid arrows indicate the enlargement direction of the structure. Detailed explanations of the processes (a) to (f) are given in the text.

#72623 - $15.00 USD
Received 3 July 2006; accepted 16 August 2006

case for $LiTaO_3$ ($\sigma_{dark} = 1.5 \times 10^{-15}\Omega^{-1}cm^{-1}$)[10], already a weak stray light can contribute to a strong widening of the photoinduced waveguide structure. Due to this widening, the probe beam was not guided anymore, which is indicated by a decrease of the monitored signal at the photodiode. Since the widening was induced by week stray light, this process was much slower than the build-up of the waveguide. In the case of the presence of background illumination, the widening is avoided due to the artificial increase of the homogeneous background conductivity.
(d) Quasi-fixed space-charge field: When the UV controlling light is blocked, the index profile does not change, it remains quasi-fixed due to charges trapped in deep traps as explained before at stage (b). These charges generate a space charge field that screens the applied field E_0. Therefore, by switching off the applied electric field, this space charge field remains and the refractive index profile increases by Δn over the whole crystal. The increase of the signal in Fig. 6 after blocking the UV controlling light can be explained by an UV induced small reversible change of the absorption constant at visible wavelengths in photorefractive crystals, known as light induced absorption[9, 10].
(e) Double waveguide: By again illuminating with the UV stripe, mobile charges are produced which screen the remained(fixed) electric field. Following the space charge field, also the refractive index decreases to its original value n_0 in the screened regions. This screening is fast in the center, forming a double waveguide (Fig. 7b), and slower in adjacent regions due to the similar process as described at stage (c). The build-up and decay times of this double waveguide with no external electric field were approximately the same as the build-up and decay of the initial waveguide.
(f) Screening of the fixed structure: After some time, the fixed space-charge electric field was completely screened and the refractive index changed back to the initial value n_0.

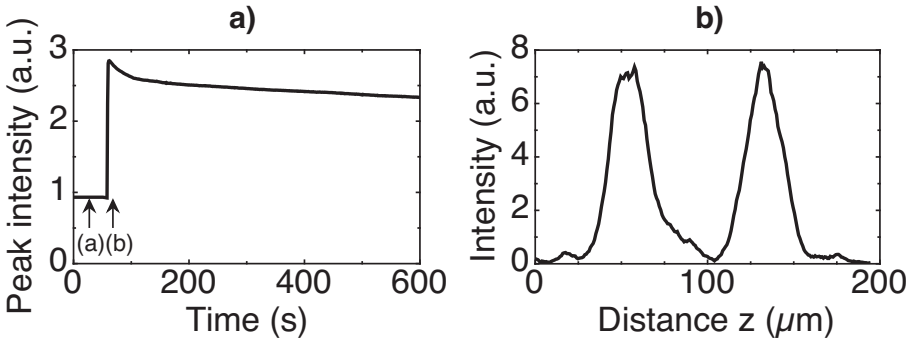

Fig. 7. a) In absence of the UV background illumination, we obtained a quasi fixed waveguide after switching off the UV controlling light just after the build-up at stage (b) of Fig. 7. The figure shows the evolution of the quasi-fixed waveguide under continuous readout. b) Beam profile of the probe light exiting the double waveguide that we obtained when switching off the UV contolling light after the fast screening at stage (e) of Fig. 7.

4. Conclusions

For the first time, to the best of our knowledge, light induced waveguides by interband photorefraction were produced in magnesium doped near-stoichiometric lithium tantalate. Guiding of the light was demonstrated for a 633 nm He-Ne probe beam with recording times of 10 ms at UV intensities of 100 mW/cm^2. The influence of the background illumination on the fast reconfigurable waveguides was demonstrated and a new fixing of the waveguide structures has been discovered: When the background UV illumination was absent, the waveguide structures

#72623 - $15.00 USD Received 3 July 2006; accepted 16 August 2006

remained fixed as soon as the controlling UV beam was blocked.

In Mg:SLT we also demonstrated fixing of holographic gratings, which we further investigated by means of interband photorefractive measurements in the transverse read-out geometry. We have shown, that the fixed structures were due to charges trapped in long-lifetime deep traps. The dark decay times were determined to be several days, while under permanent strong readout at 633 nm the structures decayed within 10 hours. The fixed grating and waveguiding structures could be deleted by illuminating the crystal homogeneously with light at wavelengths below 360 nm, in particular by the homogeneous UV background illumination.

Acknowledgements

This work has been supported by the Swiss National Science Foundation.

#72623 - $15.00 USD Received 3 July 2006; accepted 16 August 2006